Enhanced adsorption of methylene blue on chemically modified graphene nanoplatelets thanks to favorable interactions

Rabita Mohd Firdaus, Noor Izzati Md Rosli, Jaafar Ghanbaja, Brigitte Vigolo, Abdul Rahman Mohamed

J Nanopart Res vol. 21, p.257 (2019)

Doi: 10.1007/s11051-019-4701-4

Enhanced adsorption of methylene blue on chemically modified graphene nanoplatelets thanks to favorable interactions

Rabita Mohd Firdaus,[a] Noor Izzati Md Rosli,[a] Jaafar Ghanbaja,[b] Brigitte Vigolo*[b] and Abdul Rahman Mohamed*[a]

[a]School of Chemical Engineering, Engineering Campus, Universiti Sains Malaysia, 14300 Nibong Tebal, Seberang Perai Selatan, P. Pinang, Malaysia

[b]Institut Jean Lamour, CNRS-Université de Lorraine UMR 7198, Campus Artem, 2 allée André Guinier, 54011 Nancy, France

* corresponding authors :

Brigitte.Vigolo@univ-lorraine.fr (B. Vigolo); chrahman@usm.my (A. R. Mohamed)

Abstract

In the present study, the used graphene nanoplatelets (GNP) are of high structural quality offering the opportunity to modify the adsorbent/adsorbate interactions. Their chemical modification by simple acid oxidation leads to their facile dispersion in water. Morphological, structural and chemical properties of the functionalized GNP are deeply investigated by a set of complementary characterization techniques. The parametric investigation including effects

of initial concentration, contact time, solution pH and temperature of methylene blue (MB) adsorption allows to identify those being relevant for MB removal enhancement. MB adsorption is found to increase with contact time, solution temperature and acidic pH. The nature of the MB-GNP interactions and the possible adsorption mechanisms, relatively little understood, are here particularly studied. MB-GNP adsorption is shown to follow a Langmuir isotherm and a pseudo-first-order kinetic model. The adsorption capacity of MB on the chemically modified GNPs (q_m=225 mg/g) with respect to the external surface is relatively high compared to other carbon nanomaterials. Such adsorbent certainly merits further consideration for removal of other dyes and heavy metals from wastewaters.

Keywords: graphene; functionalization; interactions, adsorption; dye removal

1. Introduction

Since more than ten years, many synthesis methods have been developed leading to produce graphenic materials in large volumes (Cheng et al. 2017; Yu et al. 2017; Polat et al. 2015; Novoselov et al. 2012). Especially chemical and mechanical exfoliation of graphite allows to prepare various forms of graphene (Achee et al. 2018). This variety of graphene-based materials offers various and innovative applications which can be now advantageously envisaged with graphene. Environmental applications are especially targeted since added to their high surface area, graphenic materials can be considered as a platform man can chemically modify to generate any specific functionality. Among them depollution by contaminant adsorption has attracted high attention recently. Textile industries consume huge amounts of water and chemicals, particularly in the dyeing and finishing processes. Besides, textile industries focus primarily on colored cloth production and approximately 700,000 tons of dyes

produced per year are estimated with about 20 % of them are discharged in the effluents (Holkar et al. 2016). Discharge of highly colored synthetic dye waste could be extremely harmful to marine organisms and may even be resistant to natural biological degradation (Holkar et al. 2016; Tahir et al. 2016; Khan and Malik 2014).

Adsorption, particularly using carbon adsorbents, is a promising green decontamination alternative to eliminate the pollutants from wastewaters. The adsorptive properties of functionalized graphene has been shown to depend on its surface area (Hou et al. 2018), functional groups and π-electron system (Zhou et al. 2016) and porous structure (Gadipelli and Guo 2015). Stability, concentration, and overall quality of the carbon nanomaterial dispersion are also critical for the adsorption process, especially for elimination of organic dyes such as methylene blue (MB) (Johnson et al. 2015) or malachite green (MG) (Robati et al. 2016). Up to now, most of the works on organic dye adsorption by graphenic materials were conducted with graphene oxide (GO) or reduced GO (rGO). Presence of carboxylated-GO within a polyphenylsulfone nanofiltration membrane was shown to enhance heavy metal removal (Shukla et al. 2018). Carboxylated-GO was also efficient to eliminate MB molecules (Zhao et al. 2017). A functionalized GO-based 3D composites was used with an excellent adsorption performance for the removal of mercury ions (Kabiri et al. 2016). Qi et al. stated that polymer-based nanomaterials (polysaccharides/GO) removed well both cationic and anionic organic dyes (Qi et al. 2017). Surface modification of GO with –SH and $–NH_2$ groups were shown to increase the number of sorption sites and facilitate bonding with heavy metals, thus improving the sorption capacity in the case of MB (Chen et al. 2016). Bradder et al. reported high adsorption capacity of GO for MB and MG compared to graphite and activated carbon attributed to electrostatic attraction (Bradder et al. 2011). However, dye molecules are chemically complicated bearing hydrophobic and hydrophilic parts eventually charged depending on the pH. And the nature of dye-adsorbent intercations, which is expected to govern

the adsorption process and thus adsorption capacity, is usually not well understood. Indeed, because of the various adsorbate/adsorbent systems, the mechanisms playing the major roles in adsorption efficiency are difficult to identify and to generalize to other systems. Control the adsorbent characteristics especially its surface chemistry appears as a key aspect for enhancing the adsorption process and determining the relevant parameters impacting the adsorption effectiveness.

Two main families of graphene commercially available can be mentioned: GO having 2-5 layers and a defected structure due to the numerous functional groups it bears (Dreyer et al. 2014) and graphene flakes or graphene nanoplatelets of often more than 10 layers with a good structural quality (Ermakov et al. 2015; Wei et al. 2009; Stankovich et al. 2006; Ghosh et al. 2010). With the aim of using a well-controlled graphenic material, we have chosen to work with high quality graphene nanoplatelets (GNPs). However, the inertness of this kind of graphenic material is unfavorable to disperse it in aqueous medium. Functionalization is an efficient way to both modify surface properties and induce dispersion of carbon nanomaterials (Georgakilas et al. 2012). In this study, we have applied a simple post-synthesis method to introduce oxygen-containing functional groups onto the sidewalls of GNPs in a controlled manner. The morphological, structural and chemical characteristics of the modified GNPs through functionalization were deeply investigated by means of complementary techniques such as scanning and high-resolution transmission electron microscopy (SEM and HRTEM), thermogravimetric analysis (TGA), Raman, Fourier transform infrared (FTIR) spectroscopy and X-ray photoelectron spectroscopy (XPS). Evaluation of the modified GNPs as a potential adsorbent for the removal of MB is discussed based on analysis of the adsorption capacity using the Langmuir and Temkin isotherm models. Adsorption capacity of the GNPs is compared to other commonly investigated carbon nanomaterials (including GO, rGO and multi-walled

carbon nanotubes (MWCNTs)). Efficiency of our modified GNPs to remove MB is found to be relatively high considering the specific surface area they offer.

2. Materials and chemicals

The used raw graphene nanoplatelets (referred to as rGNP) was supplied by Universal Science Trading, Malaysia (5 μm particle size, surface area 120-150 $m^2. g^{-1}$). Sulfuric acid, H_2SO_4 (96%), nitric acid, HNO_3 (65%), ethanol (99%) and MB, used as pollutant in this study, were purchased from Sigma-Aldrich. Deionized water supplied by USF ELGA water treatment system was used to prepare all the reagents and solutions.

2.1. Preparation of functionalized GNPs.

In a typical functionalization experiment, 1 g of rGNP was placed in a dry, three-neck, round-bottomed flask, with 1:1 mixture of 78 ml of H_2SO_4 and 96 mL of HNO_3. Then, the solution was stirred for 16 h under moderate stirring (300 rpm) at 80°C. Then the mixture was sonicated in a water bath for 15 min. After that, it was filtered and washed with distilled water until the pH of the filtrate is neutral. Subsequently, the sample was dried in an oven at 110°C for 24 h. This method was repeated for volume ratio of H_2SO_4 and HNO_3 1:3 and 3:1. The treated GNP were referred to as fGNP1, fGNP2, and fGNP3 for H_2SO_4/HNO_3 ratio of 1:1, 1:3 and 3:1, respectively.

2.2. Characterization techniques

HRTEM observations were performed using a JEM-ARM 200F apparatus at 80 kV. GNP dispersions in ethanol of the raw and the fGNP were deposited on a holey carbon grid. About 25 images were taken at different locations for each sample in order to guarantee a representative description of the samples. Fast Fourier Transform (FFT) was done on selected areas. SEM of the raw and the functionalized GNP were carried out using an FEI Verios 460L

tool under extreme high resolution (XHR) with field emission. TGA was performed with a Setaram Setsys evolution 1750. Experiments were performed in dry air (flow rate 20 mL.min^{-1}) as the carrier gas and a temperature ramp of 5 °C.min^{-1} from room temperature to 900 °C. For Raman spectroscopy analysis, a Renishaw inVia Raman microscope was used with an excitation wavelength of 632.8 nm, a laser power output of 50 mW focused on the sample with an x50 objective lens. A range from 100 to 3200 cm^{-1} of Raman shift was scanned. For each sample, at least 3 spectra were recorded on different areas on the sample deposited on a glass slide. For data analysis, after subtracting a baseline, the intensity of the D or the G band corresponding to the height at the maximum intensity of the peak is used to calculate the intensity ratio I_D/I_G. For a direct comparison of the spectrum features, the intensity of the spectra is normalized to that of the G band.

For Fourier transform infrared spectroscopy, a Model Thermo Fisher Scientific Nicolet iS1O FTIR Spectroscope was used. A Malvern Zetasizer was used to measure the surface charge of the GNP samples. For the preparation of GNP dispersions, the desired amount of the raw or the modified GNP powder (concentration of 1 mg.L^{-1}) was dispersed in water using a probe sonicator for 5 min.

The surface area and pore size were evaluated by Brunauer–Emmett–Teller (BET) standard and Barrett-Johner Halenda (BJH) method respectively using an Autosorb 1C Quantachrome analyzer. The BET surface area is also known as the specific surface area (SSA).

For XPS analysis, a Kratos Axis Ultra (Kratos Analytical, U.K.) spectrometer equipped with a monochromatic Al K_α source (1486.6 eV) was used. All spectra were recorded at a 90° takeoff angle, with the analyzed area being currently about 0.7 x 0.3 mm. Survey spectra were acquired with 1.0 eV step and 160 eV analyzer pass energy and the high-resolution regions with 0.1 eV step and 20 eV pass energy (instrumental resolution better than 0.5 eV). Curve fitting was

performed using a Gaussian/Lorentzian (70/30) peak shape after Shirley's background subtraction and using X-vision 2.2.11 software.

Contact angle goniometer (Model: OCA15plus, DataPhysics) was used to evaluate the hydrophilicity (wettability by water) of the raw and functionalized GNPs. A water droplet (1 µl) was deposited onto the sample surface through a needle tip. A magnified image of water droplet was observed by a digital camera and the contact angle readings were obtained 5s after the water drop deposited on the sample surface. For each measurement of contact angle value, at least three points from different parts of the GNP, fGNP1, fGNP2 and fGNP3 were recorded and averaged.

2.3 Batch equilibrium studies

Adsorption of MB on the prepared fGNP was performed by batch equilibrium tests. The effects of MB initial concentration, contact time, solution pH and temperature on the removal were investigated. The dye solution of few milliliters was taken at regular intervals at every 5 min for 55 min of reaction and analyzed using a UV–vis spectrophotometer (Model Shimadzu UV-1800, Japan). The concentration of the treated sample was measured at a wavelength of 665 nm. The removal efficiency ξ (%) of MB at period of time, and the equilibrium adsorption capacity q_e (mg. g^{-1}) were calculated using (1) and (2), respectively:

$$\xi = \frac{C_0 - C_t}{C_0} \times 100 \qquad \text{Eq. (1)}$$

$$q_e = \frac{C_0 - C_t}{W} \times V \qquad \text{Eq. (2)}$$

Where C_O (mg. L^{-1}) is the initial MB concentration, C_t (mg. L^{-1}) is the final concentration of MB remaining at time t, V (L) and W (g) are the volume of the MB solution and the weight of the used adsorbent, respectively.

2.4 Adsorption isotherm models

From the Langmuir theory only one dye molecule is adsorbed on each adsorption site to form a monolayer (Han et al. 2017). It is then assumed that once a dye molecule occupies a site, no further adsorption can take place at that site. That means that adsorption mainly occurs on the external surface of the adsorbent having a homogeneous surface and the intermolecular forces rapidly decrease with distance. The Langmuir equation is given by (3):

$$\frac{C_e}{q_e} = \frac{1}{K_L q_m} + \frac{1}{q_m} C_e \qquad (3)$$

where q_e (mg.g^{-1}) is the maximum adsorption capacity, K_L (L.mg^{-1}) represents the Langmuir isotherm constant and C_e (mg.L^{-1}) is the dye concentration at equilibrium. The Langmuir dimensionless separation factor is defined as:

$$R_L = \frac{1}{K_L C_O} \qquad (4)$$

R_L indicates the adsorption nature to be either unfavourable if R_L>1, linear if R_L =1, favourable if 0< R_L<1 and irreversible if R_L=0.

Freundlich model describes adsorption on heterogeneous surfaces following a multilayer adsorption mechanism. It is assumed the stronger binding sites are occupied first and that the binding strength decreases with increasing the degree of site occupation. The Freundlich model equation (5) is;

$$\log q_e = \log K_F + \frac{1}{n} \log C_e \qquad (5)$$

where q_e (mg.g^{-1}) is the amount of adsorbate adsorbed per unit mass of adsorbent; K_F (L.mg^{-1}) is Freundlich isotherm constant. K_F measures the adsorption capacity of the adsorbent and 1/n reflects the strength of adsorption in the adsorption process. If value of 1/n is below one, it

indicates a normal adsorption. On the other hand, 1/n being above one indicates favorable adsorption conditions (Qiao et al. 2016). C_e is the equilibrium concentration of the adsorbate ($mg.L^{-1}$).

Temkin isotherm considers the effect of the adsorbate interaction on the adsorbent based on the uniformly distributed binding energies. It also assumes that the heat of sorption of all the molecules in the layer decreases linearly with coverage due to sorbate/sorbent interactions. The Temkin isotherm equation expressed as (Temkin and Pyzhev 1940). The Temkin model equation is:

$$q_e = B \ln A_T + B \ln C_e \qquad (6)$$

$$B = \frac{RT}{b_T} \qquad (7)$$

A_T ($L.mg^{-1}$) is the Temkin isotherm equilibrium binding constant ($L.mg^{-1}$); b_T is the Temkin isotherm constant, R the universal gas constant (8.314 $J.mol^{-1}.K^{-1}$) and B a constant related to heat of sorption ($J.mol^{-1}$).

2.5 Adsorption kinetics

The equation of pseudo first order kinetic model is expressed by the following equation (Lagergren 1898);

$$\ln(q_e - q_t) = \ln q_e - k_1 t \qquad (8)$$

where q_t ($mg.g^{-1}$) is amount of adsorbate adsorbed at time t; q_e is the amount of adsorbate adsorbed at equilibrium ($mg.g^{-1}$) and k_1 is pseudo-first-order rate constant of adsorption (min^{-1}).

The pseudo second order equation predicts the behaviour over the entire range of adsorption, and it is agreed that an adsorption mechanism being the rate controlling step (McKay and

Sweeney 1980). The equation of pseudo second order kinetic model can be expressed using equation (9):

$$\frac{t}{q_t} = \frac{1}{k_2 {q_e}^2} + \frac{t}{q_e} \qquad (9)$$

where q_e (mg.g^{-1}) is the amount of adsorbate adsorbed at equilibrium, q_t (mg.g^{-1}) is the amount of solute adsorbed per unit weight of adsorbent at time, k_2 (min^{-1}) is the rate constant of pseudo-second-order sorption. The rate parameters k_2 and q_e can be directly obtained from the intercept and slope of the plot of t/q_t versus t.

3. Result and discussion

3.1 Structural, surface and chemical characterization of the adsorbent

Many sources of graphenic materials are currently commercially available or synthesized by the researchers themselves for their utilization as adsorbent for dye removal. With the aim of providing a comprehensive analysis of the mechanisms involved in the efficiency of adsorption capacity, a deep investigation of the structural, chemical and surface properties of the used graphene nanoplatelets has been conducted. Typical SEM images of rGNP and fGNP1 are shown in figure 1. For both rGNP and fGNP1, the GNPs appear as thin platelets with of a typical size of 1-5 mm (in agreement with supplier's information); they have a clean and smooth surface and crumple edges. SEM observations of fGNP2 and fGNP3 have a similar aspect than that observed for fGNP1 (not shown).

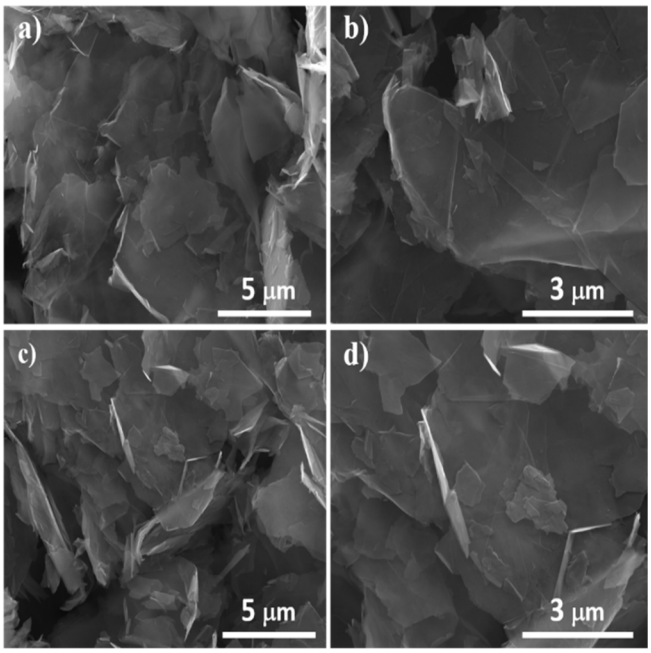

Figure 1 Typical SEM images of (a) and (b) rGNP and (c) and (d) fGNP1 at different magnifications.

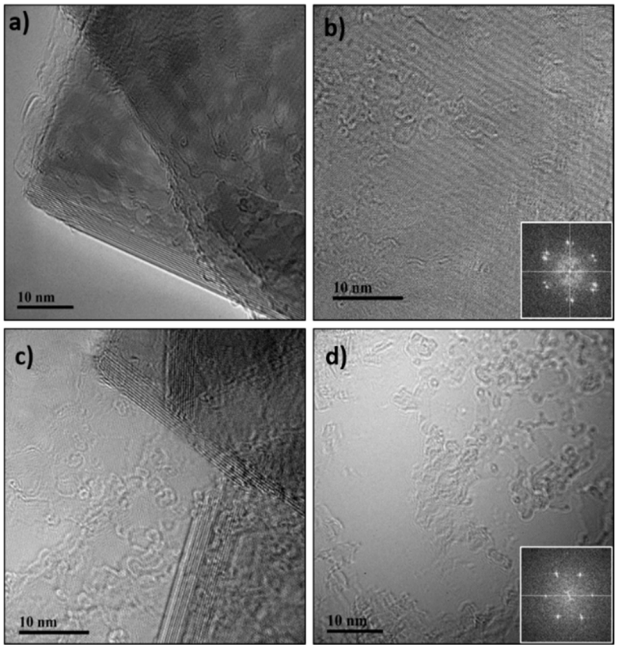

Figure 2 HRTEM micrographs of (a) and (b) rGNP and (c) and (d) fGNP1. FFT is shown for images b and d.

From HRTEM images (figure 2), GNP layers (<15 layers) were clearly observed indicating a high graphitization degree and a good structural quality of rGNP. In agreement with SEM

observations, no significant modification of the morphological characteristics is observed for fGNP1 by HRTEM. Both HRTEM and FFT images put into evidence the good quality of the basal plane of fGNP1 after the applied chemical treatment (figure 2d).

TGA was performed to analyze the thermal stability of the used GNP-based samples in an oxidative (dry air) atmosphere and the thermograms for rGNP and fGNP1 are shown in figure 3. rGNP and fGNP1 show a quite similar general shape with two main weight losses due to combustion: a weight loss of around 20 % of the sample weight in the 400-450˚C temperature range and a second weight loss of around 80 % of the sample around 650°C. The remaining mass after combustion of the carbon species above 700°C is very low (less than 1 wt.%) meaning that almost no residues remains in fGNP1 after the applied chemical treatment. This ensures that rGNP and fGNP1 are of good purity and that the prepared adsorbent is an all-carbon nanomaterial. For both samples, combustion occurs thus in two stages. The lower temperature combustion could be due to the presence of carbonaceous species of low structural quality from the GNP synthesis process itself. The main combustion temperature is not modified by the used acid-based treatment.

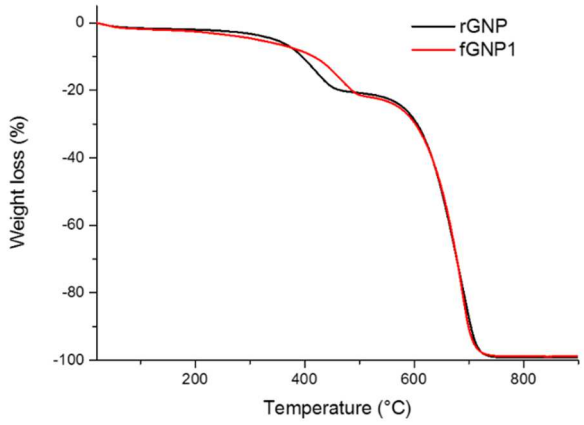

Figure 3 Thermograms under air of rGNP (black) and fGNP1 (red).

In agreement with the good structural characteristics and the number of layers (10-15 layers) observed by HRTEM, the main combustion temperature of both rGNP and fGNP1 is relatively high. The combustion of poorly ordered carbon species like amorphous carbon usually occurs below 400°C while graphite burns off above 700°C (Mercier et al. 2013). That means that the chemical method has not induced any strong modification within the layered body of the used GNP.

Commonly used as a complementary technique of HRTEM and TGA, Raman spectroscopy is a commanding method to finely probe structural modification of nanostructured carbon materials through covalent functionalization. The G band originating from the sp^2 bonded carbon atoms of the hexagonal lattice of a graphitic structure is well visible around 1585 cm^{-1}. The intensity of the D band around 1350 cm^{-1} is expected to increase when sp^2 hybridization of the carbon atoms turns to sp^3 due to functional group grafting. Figure 4 shows the Raman spectra of the GNPs before and after the used chemical treatments. In agreement with the good structural quality of the starting rGNP, its D band is relatively sharp and of weak intensity; I_D/I_G is of 0.35 for rGNP. After the applied acid-based reaction for all the used conditions, the D band is significantly more pronounced, with a larger and more intense peak. I_D/I_G of fGNP1, fGNP2 and fGNP3 are 0.91, 0.60 and 0.55, respectively. I_D/I_G increases of a factor of 1.5 or more compared to that of rGNP depending on the used acid mixture, the highest I_D/I_G being observed for fGNP1 treated with the H_2SO_4:HNO_3 ratio of 1:1. Functionalization probably occurred mainly at the edges and at the basal plane of the external layers of the GNP without any significant attack of the internal layers which leads to an increase of the I_D/I_G ratio and the preservation of their graphitic quality (from TGA and HRTEM).

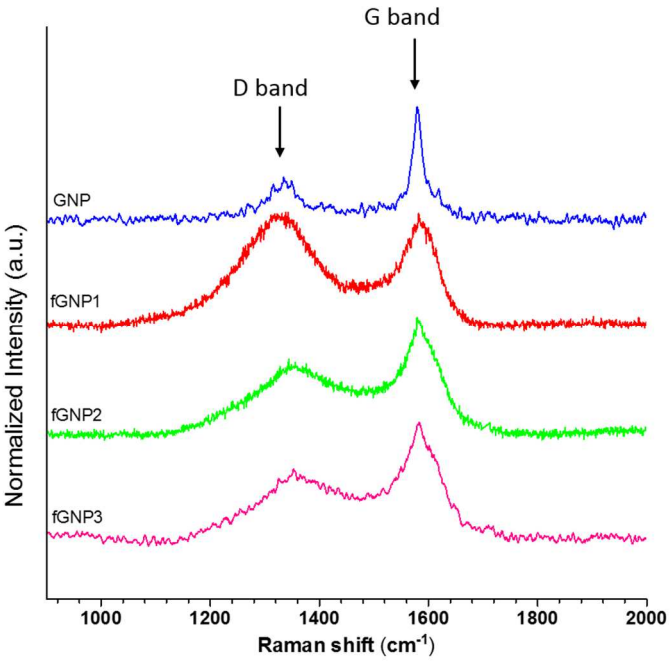

Figure 4 Raman spectra of rGNP, fGNP1, fGNP2 and fGNP3.

Presence of the oxygen containing functional groups expected to be grafted by the proposed chemical method has been investigated by FTIR. The FTIR spectra of rGNP, fGNP1, fGNP2 and fGNP3 are presented in figure 5.

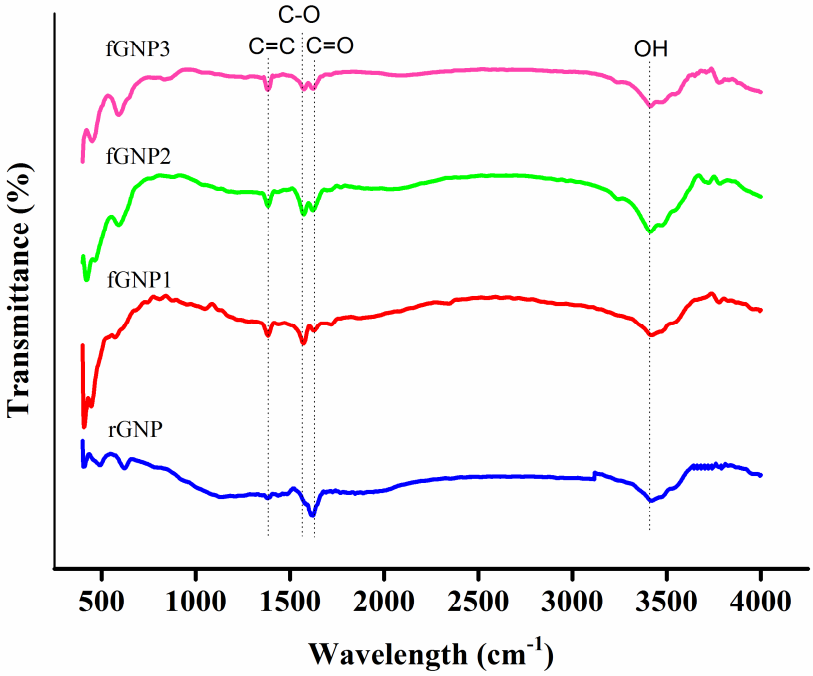

Figure 5 FTIR spectra of rGNP, fGNP1, fGNP2 and fGNP3.

The C=C stretching vibrations commonly observed around 1600 cm^{-1} for graphenic materials were well visible for all the samples. O-H stretching variations is visible for all GNP samples around 3400–3600 cm^{-1} and after functionalization C=O and C-O stretching vibrations appear in the 1720 cm^{-1} and 1570–1600 cm^{-1} range, respectively (Amiri et al. 2016). Oxygen-containing groups are evidenced in the acid treated GNP by FTIR.

From XPS analysis, O/C atomic ratio between GNP and fGNP1 (being of 3.54 and 4.89, respectively) was found to be increased of 38 % after functionalization. C1s peak of GNP and fGNP1 is shown in figure 6. The contribution at around 286 eV assigned to carbon covalently linked oxygen (contribution C1s C-O) is more pronounced for fGNP1. The area ratio between the C1s sp^2 contribution and that of the C1s C-O one for GNP and fGNP1, respectively, is of 28 % meaning that the main part of oxygen introduced in the sample by functionalization belong to oxygen-containing functions grafted to the sp^2 network of graphene.

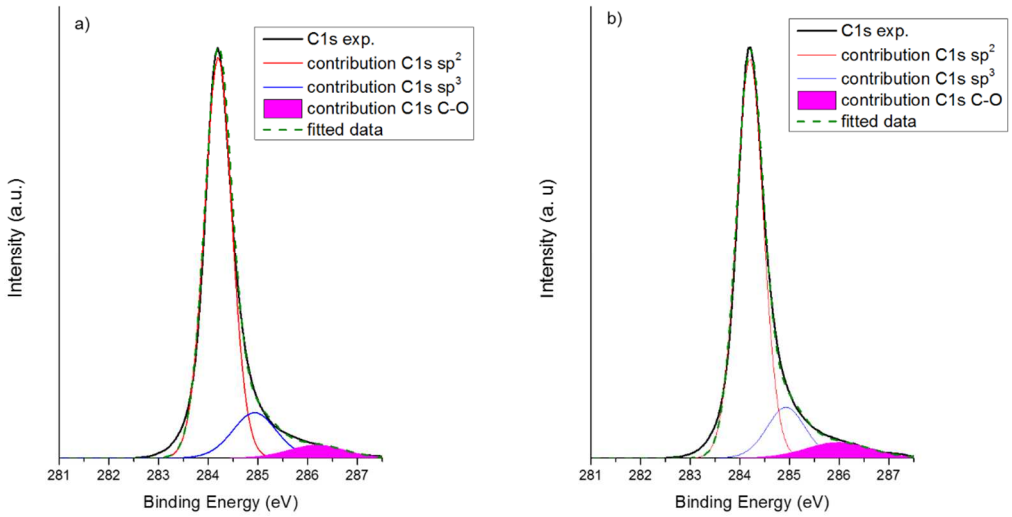

Figure 6 C1s peak from XPS for (a) GNP and (b) fGNP1.

In summary, oxygen-containing groups could be efficiently grafted at the GNP external surface by the used H_2SO_4/HNO_3 mixture. Even if carboxylic groups are most often reported for such acid attack of carbon nanomaterials, other kinds of functional groups such as lactone or carbonyl are certainly also present. Their precise nature is difficult to determine. Their hydrophilic character is however expected to play a crucial role for the efficient dispersion of the GNP and their use as MB adsorbent in water. This is the reason why fGNP1 which has shown the highest I_D/I_G ratio of the fGNP series has been chosen for the following investigations.

3.2 Improved dispersion in water

The accessible surface and the porosity properties of the used adsorbents are important factors for adsorption process of dye molecules. A porous morphology and high surface area are considered to provide more active adsorption sites leading to an enhanced adsorption uptake.

Surface area, pore volume and pore size of rGNP and fGNP1 are gathered in Table 1. In agreement with the supplier's information, for the starting rGNP sample the surface areas (BET and Langmuir) are not higher than 117 and 167 $m^2.g^{-1}$. As discussed below, these values are much lower than those usually found for other kinds of graphene such as GO for example (see Table 1). GO has usually 2-5 layers with a highly defected structure while the used GNP are composed of thick nanosheets (of 10-15 layers from HRTEM) but they are of far better structural quality. Even if the applied acid-based chemical treatment seems to only impact the external part of the GNP, it induces a significant increase of 20-40 % of all the surface properties. And the micropore volume is increased by a factor of almost 4 for fGNP1.

Table 1 Surface and porosity properties of rGNP and fGNP1.

Sample	BET surface area ($m^2.g^{-1}$)	Micropore surface area ($m^2.g^{-1}$)	Langmuir surface area ($m^2.g^{-1}$)	Micropore volume ($cm^3.g^{-1}$)
rGNP	117	53	167	0.027
fGNP1	140	73	198	0.128

High quality pristine graphene nanosheets are widely known to be highly hydrophobic due to the electron delocalization of the sp^2 network of the carbon atoms. Their dispersion in aqueous solvents is strongly compromised without any chemical modification (Hayyan et al. 2015). After having been dispersed in water, while rGNP rapidly precipitated, the dispersion of the functionalized GNPs remained relatively stable with eyes (dark solution). Zeta potential is commonly used to evaluate the colloidal stability of dispersions containing nanoparticles. In agreement with visual observations, the zeta potential of rGNP is as low as -11 mV (Table 2) meaning that the dispersion attraction forces exceed repulsion leading to poor stability (Mohandoss et al. 2017). After the performed surface functionalization, zeta potential is

significantly reduced for all the fGNP samples. It is of -44 and -48 mV for fGNP2 and fGNP3, respectively. For fGNP1, it is reduced to -59 mV. Usually, an absolute value of a zeta potential of 40-60 mV is found for high stable dispersions (Ali et al. 2018). The applied chemical treatments could increase affinity between GNP surface and the MB solution through grafting of oxygenated functional groups inducing a good dispersibility of fGNP.

Table 2 Zeta Potential values for rGNP, fGNP1, fGNP2 and fGNP3 dispersed in water

Samples	Zeta potential (mV)
rGNP	- 11
fGNP1	- 59
fGNP2	- 44
fGNP3	- 48

3.3 Hydrophilicity by water

Figure 7a shows the contact angle of a water droplet of raw GNP compared to the functionalized GNP (figs. 7b-7d). The contact angle of GNP decreased from ~58° down to ~23° with the hydrophilic nature of the grafted moieties at the GNP sheet surface for GNP and fGNP1, respectively. The contact angle for fGNP2 and fGNP3 was approximately ~35° and ~40°, respectively.

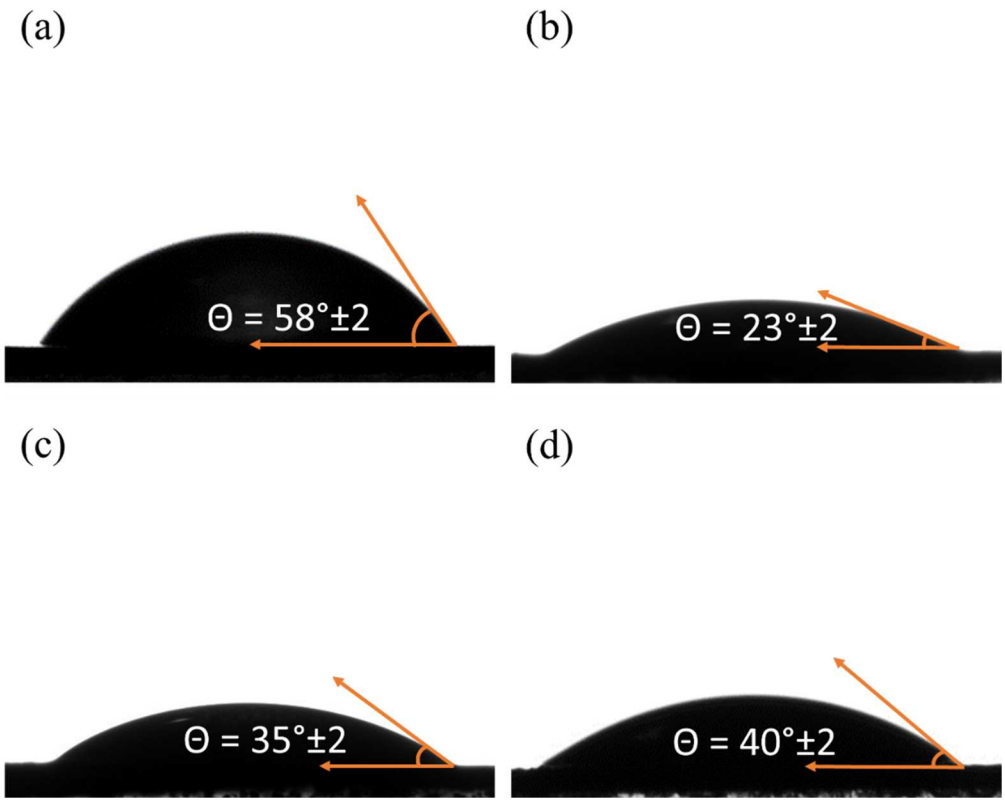

Figure 7 Contact angle measurements of aqueous dispersions of (a) GNP, (b) fGNP1, (c) fGNP2 (d) fGNP3.

3.4 Effect of adsorption parameters on MB removal

Among the parameters playing the major role in dye adsorption capacity, initial concentration, contact time, tempearture and pH are known to be relevant. To follow MB adsorption, UV-vis absorption spectra of the MB solution placed in contact with the raw and the functionalized GNP (rGNP and fGNP1) were recorded after the chosen contact time. Figure 8 shows the evolution of the absorbed intensity in the visible spectral domain of the MB solutions with increasing the contact time with the adsorbent.

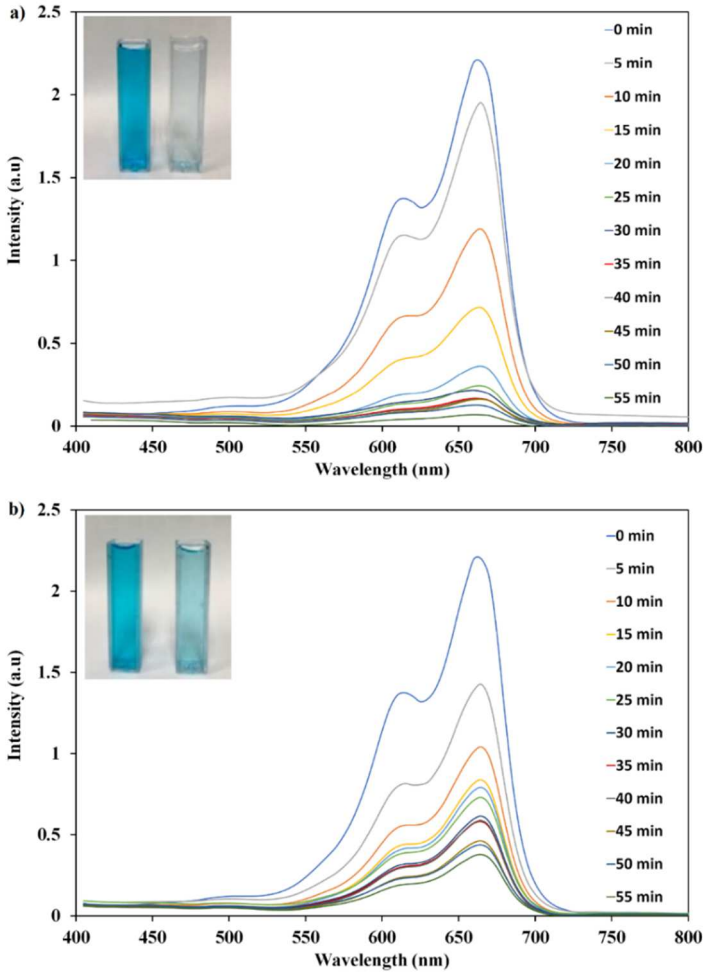

Figure 8 UV-vis absorption spectra after various contact times of MB (a) with fGNP1 and (b) rGNP. Insert: aspect of the MB solution in the UV-visible cell after a contact time t=0 (left) and t=55 min (right) with (a) fGNP1 and with (b) rGNP1, respectively.

After a contact time of 55 min, the disappearance of the blue color of MB by fGNP1 is obvious leading to an almost colorless solution contrary to with rGNP used as adsorbent. For all the samples, the absorption spectra show a similar shape with two broad peaks at around 605 and 665 nm. The evolution of the intensity of the absorbed intensity as a function of the contact time is analyzed in the following section by using the most intense peak (at 665 nm) to determine the MB removal rate.

3.4.1 Effect of MB initial concentration and contact time on adsorption equilibrium

Batch adsorption of MB from aqueous solution was carried out, while the initial dye concentration was varied in the range of (25-200) $mg.L^{-1}$. Figure 9 shows the effects of MB initial concentration and contact time against the MB removal for both rGNP and fGNP1 at 60 °C. As normally observed, MB removal increases as a function of contact time for rGNP and fGNP1. For all the conditions and both adsorbents, the adsorption process is of greatest rate at the beginning, i.e. for short contact times. As the contact time increases, MB adsorption rate slows down much more rapidly for rGNP than for fGNP1 which shows a continuous increase of the MB adsorption until 45 min of contact time for all the used initial concentrations. At the preliminary stage of adsorption, the accessibility of vacant surface sites is favored and after a certain time period, the number of occupied sites increases and repulsive forces certainly appear between the adsorbed MB and the MB remaining in the bulk phase (Banerjee and Chattopadhyaya 2017). The equilibrium time is reached at around 45 min for both adsorbents and all the used conditions. Depending on the MB initial concentration, the maximum of adsorption efficiency is in the 53-65 % and 76-88 % range for rGNP and fGNP1, respectively.

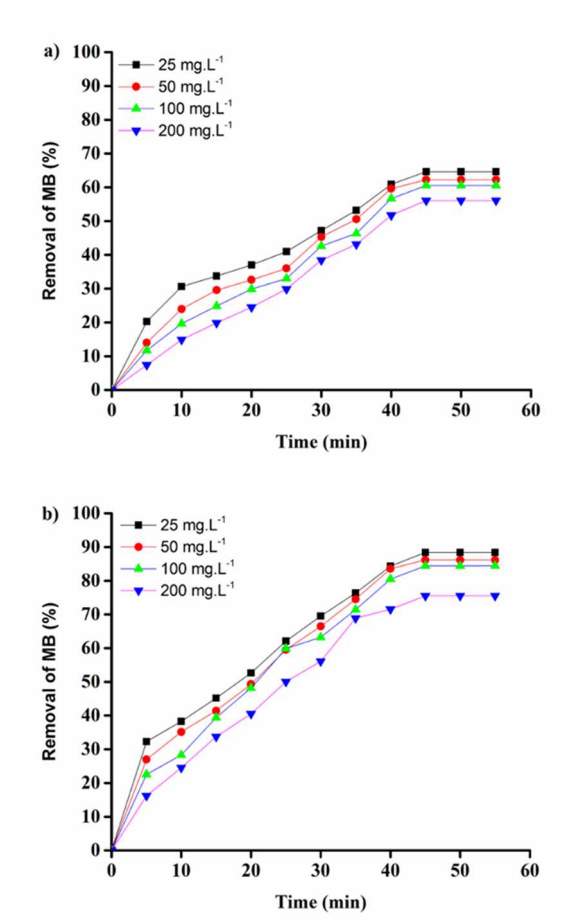

Figure 9 Variation of MB removal with respect to time of (a) rGNP and (b) fGNP1 at pH = 4 and T = 60 °C.

However, increasing in dye concentration leads to a continuous decrease in adsorption for both rGNP and fGNP1, as normally observed. fGNP1 shows significantly higher adsorbent properties with a maximum of MB removal of 87 % compared to 65 % for rGNP at 25 $mg.L^{-1}$ of initial concentration of MB. An improvement of more than 27 % is therefore achieved after GNP functionalization. The functionalization reaction has certainly several effects that are possibly combined to reach the high removal MB efficiency obtained for our adsorbent. Even if it is limited, the functionalization process could induce structural damaging increasing the intrinsic surface area of fGNP1 compared to rGNP. The grafted oxygen-containing functional groups are responsible for the observed better dispersion of the modified GNP which offer as

well higher accessible surface for dye adsorption. The GNP being more hydrophilic, they have a better affinity with MB. The maximum MB removal efficiency by fGNP1 is consequently as high as 87 % leading to a highly efficient adsorbent.

3.4.2 Effect of solution pH on MB adsorption

pH is a key factor for adsorption processes especially for carboxylated carbon nanomaterials since their surface properties highly depend on the pH in the surrounding water. The resulted interactions between MB, having both charged and hydrophobic parts, are expected to be modified through pH modification. Figure 10 shows the effect of solution pH on the MB removal by fGNP1. The highest MB adsorption by fGNP1 was achieved at pH 4, with MB removal as high as 88.42 %, at MB initial concentration of 100 $mg.L^{-1}$. In aqueous medium, MB shows a pKa of 5.8 indicating that it can exist in the molecular form when the pH < pKa and ionized form when the pH > pKa (Zazouli et al. 2016). Carboxylic acid groups at the GNP surface are negatively charged above pH 4-5 (COOH pKa), meaning that at low pH, for which MB adsorption is high, GNP surface is probably not charged. Moreover, contrary to GO, the functionalization level is here rather low since it could be estimated from Temperature-programmed desorption (TPD) to be around 1 functional groups every 6 C_6-ring of GNP in average (cf. Supporting Information, Fig. S1). Even if we consider that the used GNPs are rather thick and that the functional groups are mainly situated at the external surface of the nanoplatelets (more reactive sites), it is likely to find hydrophobic zones under the form of sp^2 non-oxidized domains on the basal plane of the functionalized GNPs. Since the MB molecule has two aromatic rings with π electrons, MB-fGNP interactions can be here mostly governed by π–π stacking; hydrophobic intercations being thus the primary driving force for adsorption in the low pH domain (Li et al. 2013a; Lv et al. 2018; Qi et al. 2018; He et al. 2018). Electrostatic interactions probably become predominant in MB adsorption at higher pH when COOH are

deprotonated. These negatively charged sites on fGNP basal plane could lead to attractive forces (even if they seem of less intensity than hydrophobic forces) with the positively charged MB especially above pH 5.8 corresponding to MB pKa (Kaya et al. 2018). These two effects contribute to the rather good MB adsorption on fGNP1 surface over a wide pH range.

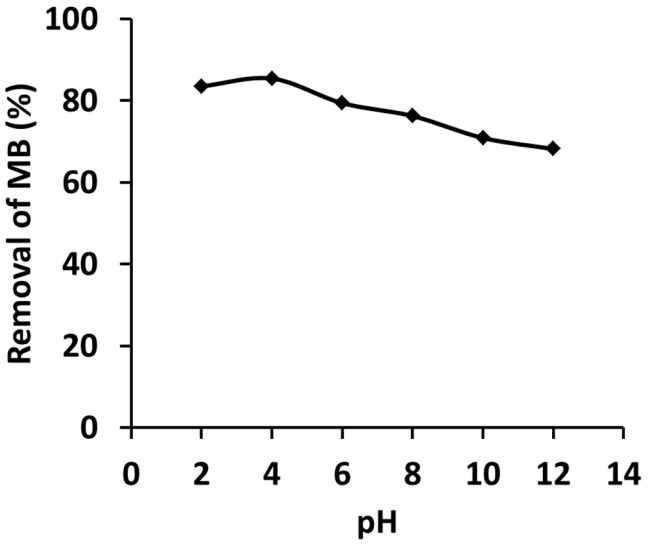

Figure 10 Effect of pH on MB removal efficiency at C_0 = 200 mg.L^{-1} and T = 60 °C.

3.3.3 Effect of solution temperature on MB adsorption

Temperature usually has a significant effect on the adsorption process, as any temperature change may affect the adsorption equilibrium (Kushwaha et al. 2017). When the adsorption capacity increases with an increase in temperature, it indicates that the adsorption process is endothermic (Pathania et al. 2017). For this study, three different temperatures (30, 45 and 60˚C) were chosen to investigate their effect on MB adsorption. Figure 11 shows the effect of solution temperature on rGNP and fGNP1 adsorption capacity.

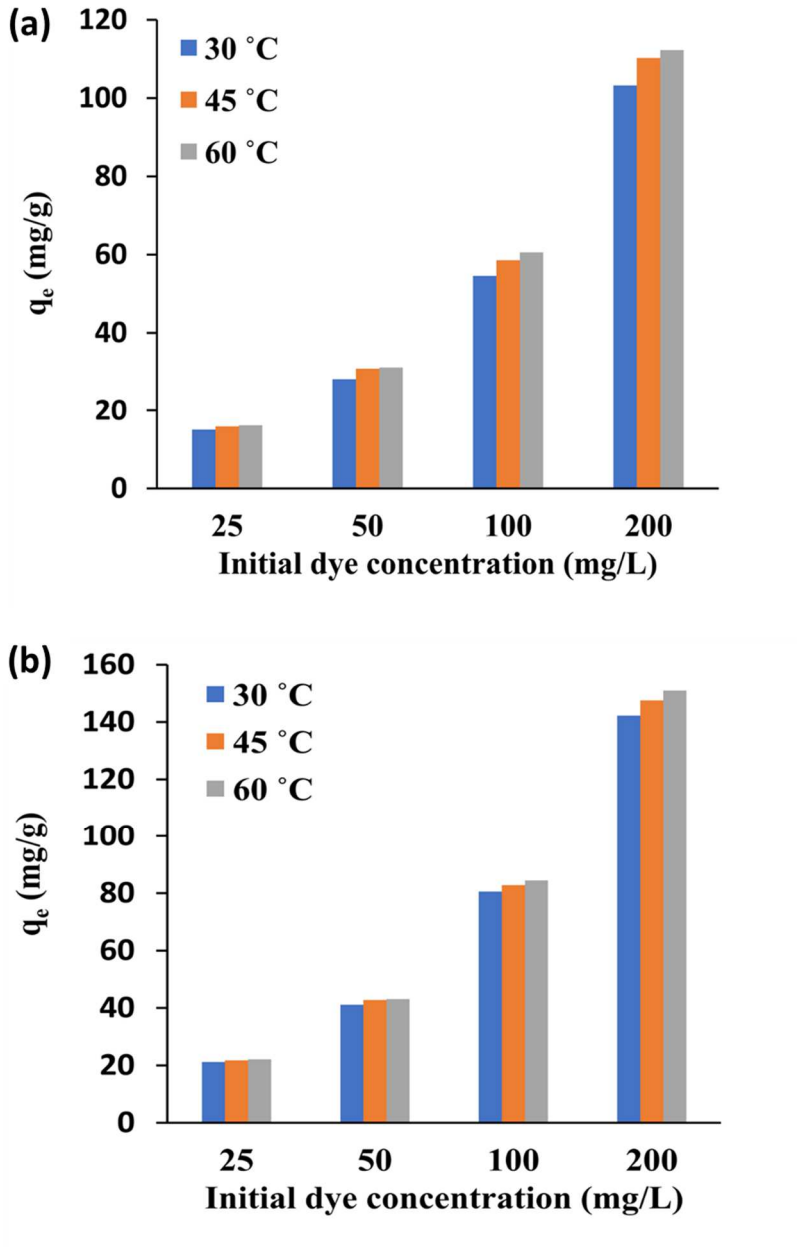

Figure 11 Effect of temperature on the adsorption capacity of (a) rGNP and (b) fGNP1 at C_0 = 200 mg.L^{-1} and pH 4

Based on the results obtained, for rGNP, when the temperature rises from 30 to 60 ˚C, the amount of adsorbed MB is increased from 15 to 130 mg.g^{-1}, from 16 to 110 mg.g^{-1} and from 16 to 112 mg.g^{-1} at 30, 45 and 60˚C, respectivly. For fGNP1, when the temperature increases from

30 to 60 ˚C, the amount of adsorbed MB is incaresed from 21 to 142 mg.g^{-1}, from 22 to 147 mg.g^{-1} and from 22 to 151 mg.g^{-1} at 30, 45 and 60 ˚C, respectively. The MB adsorption by both rGNP and fGNP1 is thus an endothermic process. When temperature increases, dye mobility increases enhancing that way its interaction with the active sites of the adsorbent surface (Banerjee and Chattopadhyaya 2017).

3.5 Adsorption isotherm study of MB adsorption on the chemically modified graphene nanoplatelets

In this study, the linear forms of the isotherm models of Langmuir, Freundlich and Temkin were investigated at 30, 45 and 60 ˚C. Figure 12 shows the determined separation factor R_L versus the initial concentration of MB for its adsorption on fGNP1. The R_L values are in the 0-1 range confirming that the adsorption of MB on the modified GNPs is favorable for the used concentration ranges, *i.e.* 25, 50, 100 and 200 mg.L^{-1}.

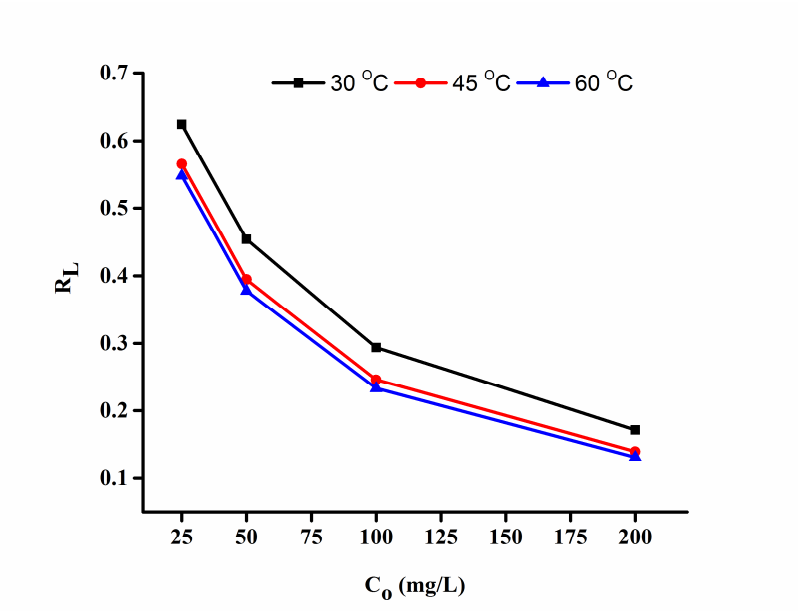

Figure 12 Separation factor (R_L) as a function of the initial concentration of MB for its adsorption on fGNP1 at 30, 45 and 60 °C.

Table 3 summarizes all the three isotherm model constants and correlation coefficients for MB adsorption onto fGNP1 adsorbent. For all the temperatures, R^2 being higher for Langmuir than for Freundlich and Temkin models (Langmuir > Freundlich > Temkin), Langmuir adsorption better describes MB adsorption isotherms. MB monolayer coverage mainly occurs on the outer surface of the functionalized GNPs. In addition, this result also compliments to the error function analysis where the calculated value of χ^2 gained is between 0.030 and 0.045, which is the lowest among the three isotherm models. Freundlich 1/n constant is found to be above 1 indicating also a favorable adsorption for our MB/GNP1 system. Moreover, in agreement with MB adsorption evolution with temperature (Fig. 10), the adsorption reaction is endothermic since B value from Temkin analysis is positive.

Table 3 Langmuir, Freundlich and Temkin isotherm model constants and correlation coefficients.

Isotherms	Solution temperature (°C)	Constants				R^2
		Q_m (mg. g^{-1})	K_L ($L.mg^{-1}$)	R_L	χ^2	
Langmuir	30	245.5	0.024	0.62	0.0453	0.9943
	45	239.0	0.030	0.57	0.0039	0.9996
	60	244.0	0.033	0.55	0.0431	0.9955
		Constants				
Isotherms	Solution temperature (°C)	K_F (mg. g^{-1} $(L.mg^{-1})^{1/n}$)	1/n	-	χ^2	R^2
Freundlich	30	8.60	1.40	-	0.5604	0.9875
	45	10.5	1.46	-	0.5294	0.9874
	60	11.3	1.46	-	0.5902	0.9155

Isotherms	Solution temperature (°C)	Constants				
		A_T ($L.mg^{-1}$)	B	-	χ^2	R^2
Temkin	30	0.34	45.50	-	18.3941	0.8777
	45	0.34	45.50	-	19.2134	0.9104
	60	0.45	46.55	-	19.9450	0.9155

3.6 Kinetic analysis of MB adsorption on the chemically modified graphene nanoplatelets

Adsorption kinetic study is important for water treatment since it provides valuable information on reaction pathways and the adsorption mechanisms. It determines how the adsorption rates depends on the initial concentration of the adsorbate in solution and how the rates are affected by the adsorption capacity or the adsorbent characteristics.

Tables 4 lists the results of the rate constants from analysis by the pseudo first order and pseudo second order model for different initial MB concentrations at temperature 30, 45, and 60 °C. MB adsorption on the carboxylated GNPs is then better represented by the pseudo-first-order kinetic model since the calculated q_e value is found to be closer to the experimental q_e in agreement with the high correlation number found (R^2 of around 0.98). This study indicates that the MB-fGNP1 adsoprtion is more inclined towards physisorption, as expected.

Table 4 Kinetic parameters and coefficients for the pseudo-first-order and pseudo-second-order model applied to MB adsorption on the functionalized GNP surface.

Temperature (˚C)	Kinetic Model	Kinetic parameter	Initial dye concentration (mg/L)			
			25	50	100	200
		$q_{e\ exp}$ (mg/g)	21.1666	41.1342	80.5659	142.2466
30		$q_{e\ cal}$	20.5315	40.1082	78.1925	140.9537

	Pseudo-first order	k_1	2.9402	3.0791	2.9570	2.6095
		R^2	0.9797	0.9758	0.9790	0.9739
	Pseudo-second order	$q_{e\ cal}$	15.1411	37.3081	70.1280	126.3690
		k_2	0.0384	0.0157	0.0043	0.0013
		R^2	0.8726	0.8979	0.7642	0.5612
	order	$q_{e\ cal}$	19.5315	40.1082	81.1925	143.9537
		k_1	3.2022	3.0229	2.8384	3.4852
		R^2	0.9163	0.9264	0.9781	0.8767
	Pseudo-second order	$q_{e\ cal}$	17.5633	38.4097	78.7495	130.6191
		k_2	0.0675	0.0277	0.0085	0.0026
		R^2	0.8891	0.8631	0.9359	0.6822
60	Pseudo-first order	$q_{e\ cal}$	19.0929	40.6385	82.3589	146.6760
		k_1	3.0246	3.1292	3.1007	3.8599
		R^2	0.9484	0.9433	0.9677	0.8634
	Pseudo-second order	$q_{e\ cal}$	17.6706	37.8400	76.3371	130.6016
		k_2	2.5943	1.0850	0.2666	0.0972
		R^2	0.7939	0.7518	0.7031	0.6291

3.7 MB-fGNP interaction forces and adsorption capacity

Parametric, thermodynamic and kinetic investigations have shown that adsorption of MB on the chemically modified GNPs is remarkably favorable. To develop interesting materials for pollutant removal, the adsorption capacity is one of the major parameters to assess the removal efficiency. As mentioned, a lot of adsorbent-adsorbate systems can be found in literature. They can be very different in nature and their adsorption capacity are difficult to compare. Among the reported results, MB is often used as a standard to study development of decontaminating

systems of water. Table 5 gathers findings reported for nanocarbon-based adsorbents developed for MB removal and for which adsorption isotherms can be well fitted with the Langmuir model.

Table 5 Adsorption capacity (q_m calculated from Langmuir model) of MB adsorbed by various nanomaterials and the used parameters, SSA and q_m/SSA

Adsor-bent	Experimental conditions					SSA ($m^2.g^{-1}$)	q_m/SSA (mg of MB.c m^{-2})	Ref.
	Concentration ($mg.L^{-1}$)	Temperature (˚C)	Time (min)	pH	q_m ($mg.g^{-1}$)			
MWCNT	20-60	50	60	10	95.2	119	0.8	(Selen et al. 2016)
MWCNT	15-50	60	any time	7	64.7	N.A.	-	(Yao et al. 2010)
MWCNT	5-300	22	480	6.9-7.9	400	358	1.1	(Szlachta and Wójtowicz 2013)
MWCNT	8-25	50	180	6.4-9.4	N.A.	N.A.	-	(Zhao et al. 2013)
GO	20-70	25	500	5.4	181.81	N.A.	-	(Li et al. 2013b)
GO	45	60	600	9-10	306.5	N.A.	-	(Guo et al. 2016)
rGO	10-50	10	180	7	339	270	1.3	(Chen et al. 2013)
rGO	20-100	60	1300	10	204.08	296	0.7	(Liu et al. 2012)
fGNP1	25-200	60	55	4	224.62	140	1.6	this work

The maximum adsorption capacity (q_m) of our modified GNP is rather good but it is lower than most of the GO or rGO reported. As already discussed, our fGNP1 is composed of relatively thick platelets compared to GO or rGO, for example and its SSA can be quite low compared to that reported for MWCNTs, GO and rGO depending on the sample source. The adsorption process is mainly governed by interactions between the adsorbate and the surface of the adsorbent. This is the reason why it is interesting to compare the adsorption capacity related to the SSA of the adsorbent. This value can be simply calculated by dividing the adsorption capacity (q_m) by the corresponding SSA for each carbon nanomaterial (Table 5). q_m/SSA corresponds therefore to the amount of MB adsorbed per cm^2 of the used nanomaterials. MB removal efficiency per surface unit for our modified GNP is significantly higher meaning that the involved interactions between MB and the functionalized GNP are strongly favorable leading to an effective adsorption, in agreement with the thermodynamic and kinetic studies. From the literature, there is no agreement regarding which type of interaction (electrostatic, π-π stacking, van der Waals, hydrophobic, hydrogen bonding) is favorable for each kind of adsorbent. GO for example bears a lot of functional groups such as carboxylic acids that can easily release protons in water leading to an adsorbent surface charged (Dimiev et al. 2012). In that case, adsorption is likely to be governed by electrostatic interactions. For the prepared modified GNPs, we have shown that at low pH, hydrophobic forces could be rather involved in the adsorption process (Hu et al. 2013). Hydrophobic interactions are shown here to play a significant role in the observed favorable interactions between MB and fGNP1.

Based on the possible functional groups present at the surface of fGNP1, MB adsorption could follow three mechanisms depending on the adsorption site (Figure 13) (Pérez-Ramírez et al. 2016). First, interaction between the carboxyl groups of fGNP1 and MB could be electrostatic (Figure 13 (a)). The positively charged MB molecules could strongly react on the surface of fGNP1 with the negative charge of the dissociated form of carboxyl groups (Nassar

et al. 2015; Yusuf et al. 2015). Second, adsorption by hydrogen bonding could occur between the hydrogen or oxygen of the possible epoxide, carboxyl, hydroxyl, carbonyl, etc… groups introduced at fGNP1 surface and oxygen/nitrogen or hydrogen of the MB molecule, respectively (Figure 13 (b)). Thirdly, π-π interactions are possible between the preserved parts of the GNP surface and the aromatic ring of the dye molecules (Figure 13 (c)). Adsorption was here also probably enhanced by the combination of synergetic effects of all adsorption mechanisms leading to high efficiency of MB dye removal by the chemically functionalized GNP (Lan Huong et al. 2018).

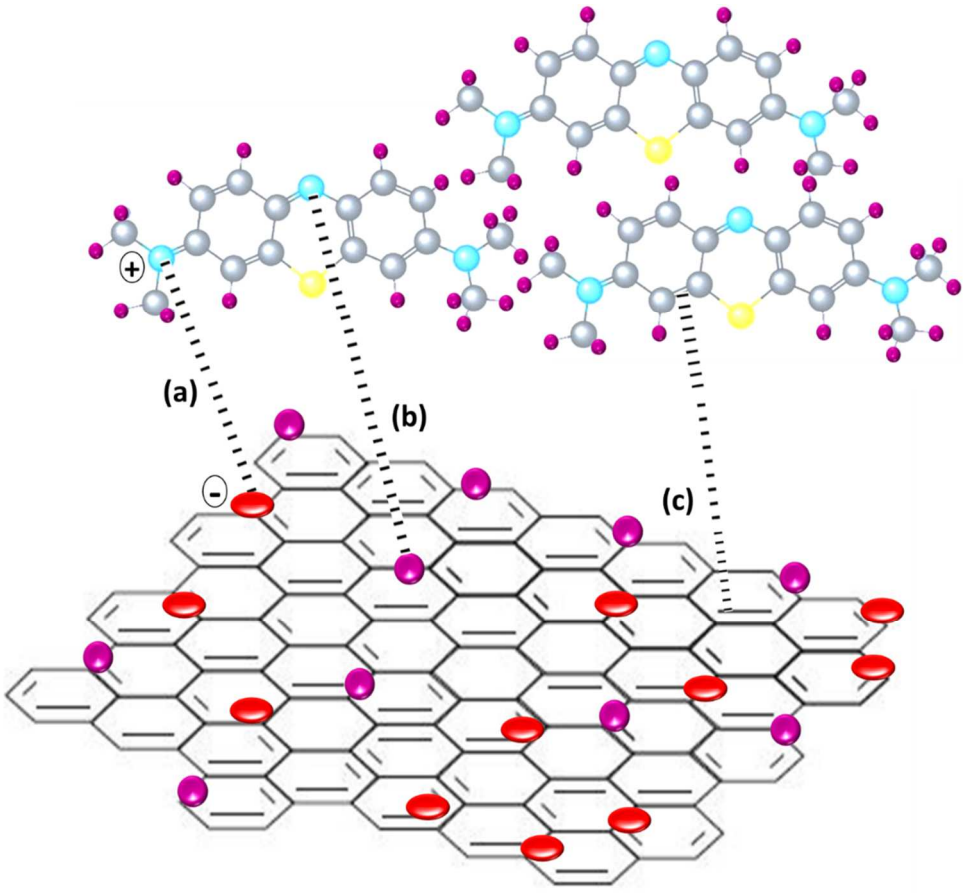

Figure 13 Schematic representation of MB adsorption on the fGNP1 surface: (red: oxygen); (purple: hydrogen) ;(blue: nitrogen);(yellow: sulfur).

4. Conclusion

This work investigates graphene nanoplatelets of high structural quality; this carbon nanomaterial is seldom studied for its ability to adsorb pollutants. A challenge resides in the success of functionalization for their facile dispersion in aqueous medium. The occurrence of functionalization at the external layers of our graphene nanoplatelets was evidenced by means of several complementary characterization methods. The applied chemical method which allows grafting oxygen-containing functional groups at the graphene surface is quite simple. Their facile dispersion in water offers favorable conditions for an efficient adsorption of methylene blue. The complete parametric study has allowed to better understand the MB/GNP interactions. Adsorption isotherms could be well fitted with the Langmuir model. Also, the best fit was obtained with a pseudo-first-order kinetic model. Interestingly, compared to other carbon nanomaterials, the adsorption capacity related to the respective surface area of these graphene nanoplatelets is significantly higher. Our findings highlight the importance of hydrophobic interactions for dye adsorption already reported in literature. These results suggest that such nanomaterials have a great potential to be used as contaminant adsorbents in wastewater treatment.

Conflicts of interest

There are no conflicts to declare

Acknowledgments

The authors would like to thank Lionel Aranda for his help for TGA experiment. They also thank Ms. Nawal Berrada and Dr. Alexandre Desforges for the fruitful discussions. We thank Dr. M. Mallet and Mr. A. Renard from the spectroscopy and microscopy Core Facility of SMI

LCPME (Université de Lorraine-CNRS–http://www.lcpme.cnr-nancy.fr). The authors thank the French Ambassy in Malaysia for financial support especially for Ms. R. Mohd Firdaus' Fellowship. We acknowledge the financial support given by the Ministry of Education Malaysia through Universiti Sains Malaysia-NanoMITE (203/PJKIMIA/6720009) and Institute of Postgraduate Studies, Universiti Sains Malaysia.

References

Achee TC, Sun W, Hope JT, Quitzau SG, Sweeney CB, Shah SA, Habib T, Green MJ (2018) High-yield scalable graphene nanosheet production from compressed graphite using electrochemical exfoliation. Scientific Reports 8 (1):14525. doi:10.1038/s41598-018-32741-3

Ali N, Teixeira JA, Addali A (2018) A Review on Nanofluids: Fabrication, Stability, and Thermophysical Properties. Journal of Nanomaterials 2018:33. doi:10.1155/2018/6978130

Amiri A, Shanbedi M, Ahmadi G, Eshghi H, Kazi SN, Chew BT, Savari M, Zubir MNM (2016) Mass production of highly-porous graphene for high-performance supercapacitors. Scientific Reports 6:32686. doi:10.1038/srep32686

https://www.nature.com/articles/srep32686#supplementary-information

Banerjee S, Chattopadhyaya MC (2017) Adsorption characteristics for the removal of a toxic dye, tartrazine from aqueous solutions by a low cost agricultural by-product. Arabian Journal of Chemistry 10:S1629-S1638. doi:https://doi.org/10.1016/j.arabjc.2013.06.005

Bradder P, Ling SK, Wang S, Liu S (2011) Dye Adsorption on Layered Graphite Oxide. Journal of Chemical & Engineering Data 56 (1):138-141. doi:10.1021/je101049g

Chen D, Zhang H, Yang K, Wang H (2016) Functionalization of 4-aminothiophenol and 3-aminopropyltriethoxysilane with graphene oxide for potential dye and copper removal. Journal of Hazardous Materials 310:179-187. doi:https://doi.org/10.1016/j.jhazmat.2016.02.040

Chen L, Yang J, Zeng X, Zhang L, Yuan W (2013) Adsorption of methylene blue in water by reduced graphene oxide: Effect of functional groups. Materials Express 3 (4):281-290

Cheng Y, Zhou S, Hu P, Zhao G, Li Y, Zhang X, Han W (2017) Enhanced mechanical, thermal, and electric properties of graphene aerogels via supercritical ethanol drying and high-temperature thermal reduction. Scientific Reports 7 (1):1439. doi:10.1038/s41598-017-01601-x

Dimiev AM, Alemany LB, Tour JM (2012) Graphene oxide. Origin of acidity, its instability in water, and a new dynamic structural model. ACS Nano 7 (1):576-588

Dreyer DR, Todd AD, Bielawski CW (2014) Harnessing the chemistry of graphene oxide. Chemical Society Reviews 43 (15):5288-5301

Ermakov VA, Alaferdov AV, Vaz AR, Perim E, Autreto PAS, Paupitz R, Galvao DS, Moshkalev SA (2015) Burning Graphene Layer-by-Layer. Scientific Reports 5:11546. doi:10.1038/srep11546

https://www.nature.com/articles/srep11546#supplementary-information

Gadipelli S, Guo ZX (2015) Graphene-based materials: Synthesis and gas sorption, storage and separation. Progress in Materials Science 69:1-60. doi:https://doi.org/10.1016/j.pmatsci.2014.10.004

Georgakilas V, Otyepka M, Bourlinos AB, Chandra V, Kim N, Kemp KC, Hobza P, Zboril R, Kim KS (2012) Functionalization of Graphene: Covalent and Non-Covalent Approaches, Derivatives and Applications. Chemical Reviews 112 (11):6156-6214. doi:10.1021/cr3000412

Ghosh S, Bao W, Nika DL, Subrina S, Pokatilov EP, Lau CN, Balandin AA (2010) Dimensional crossover of thermal transport in few-layer graphene. Nature materials 9 (7):555

Guo Y, Deng J, Zhu J, Zhou X, Bai R (2016) Removal of mercury (II) and methylene blue from a wastewater environment with magnetic graphene oxide: adsorption kinetics, isotherms and mechanism. RSC Advances 6 (86):82523-82536

Han S, Liu K, Hu L, Teng F, Yu P, Zhu Y (2017) Superior Adsorption and Regenerable Dye Adsorbent Based on Flower-Like Molybdenum Disulfide Nanostructure. Scientific Reports 7:43599. doi:10.1038/srep43599

Hayyan M, Abo-Hamad A, AlSaadi MA, Hashim MA (2015) Functionalization of graphene using deep eutectic solvents. Nanoscale Research Letters 10 (1):324. doi:10.1186/s11671-015-1004-2

He J, Cui A, Deng S, Chen JP (2018) Treatment of methylene blue containing wastewater by a cost-effective micro-scale biochar/polysulfone mixed matrix hollow fiber membrane: Performance and mechanism studies. Journal of colloid and interface science 512:190-197

Holkar CR, Jadhav AJ, Pinjari DV, Mahamuni NM, Pandit AB (2016) A critical review on textile wastewater treatments: possible approaches. Journal of environmental management 182:351-366

Hou D, Liu Q, Wang X, Quan Y, Qiao Z, Yu L, Ding S (2018) Facile synthesis of graphene via reduction of graphene oxide by artemisinin in ethanol. Journal of Materiomics. doi:https://doi.org/10.1016/j.jmat.2018.01.002

Hu Y, Guo T, Ye X, Li Q, Guo M, Liu H, Wu Z (2013) Dye adsorption by resins: effect of ionic strength on hydrophobic and electrostatic interactions. Chemical Engineering Journal 228:392-397

Johnson DW, Dobson BP, Coleman KS (2015) A manufacturing perspective on graphene dispersions. Current Opinion in Colloid & Interface Science 20 (5):367-382. doi:https://doi.org/10.1016/j.cocis.2015.11.004

Kabiri S, Tran DN, Cole MA, Losic D (2016) Functionalized three-dimensional (3D) graphene composite for high efficiency removal of mercury. Environmental Science: Water Research & Technology 2 (2):390-402

Kaya NS, Yadav A, Wehrhold M, Zuccaro L, Balasubramanian K (2018) Binding Kinetics of Methylene Blue on Monolayer Graphene Investigated by Multiparameter Surface Plasmon Resonance. ACS Omega 3 (7):7133-7140. doi:10.1021/acsomega.8b00689

Khan S, Malik A (2014) Environmental and health effects of textile industry wastewater. In: Environmental deterioration and human health. Springer, pp 55-71

Kushwaha AK, Gupta N, Chattopadhyaya MC (2017) Adsorption behavior of lead onto a new class of functionalized silica gel. Arabian Journal of Chemistry 10:S81-S89. doi:https://doi.org/10.1016/j.arabjc.2012.06.010

Lagergren S (1898) Zur theorie der sogenannten adsorption geloster stoffe. Kungliga svenska vetenskapsakademiens Handlingar 24:1-39

Lan Huong PT, Tu N, Lan H, Thang LH, Van Quy N, Tuan PA, Dinh NX, Phan VN, Le A-T (2018) Functional manganese ferrite/graphene oxide nanocomposites: effects of graphene oxide on the adsorption mechanisms of organic MB dye and inorganic As(v) ions from aqueous solution. RSC Advances 8 (22):12376-12389. doi:10.1039/C8RA00270C

Li Y-H, Du Q, Tonghao L, Peng X, Wang J, Sun J, Wang Y, Wu S, Wang Z, Xia Y, Xia L (2013a) Comparative study of methylene blue dye adsorption onto activated carbon, graphene oxide, and carbon nanotubes, vol 91. doi:10.1016/j.cherd.2012.07.007

Li Y, Du Q, Liu T, Sun J, Wang Y, Wu S, Wang Z, Xia Y, Xia L (2013b) Methylene blue adsorption on graphene oxide/calcium alginate composites. Carbohydrate polymers 95 (1):501-507

Liu T, Li Y, Du Q, Sun J, Jiao Y, Yang G, Wang Z, Xia Y, Zhang W, Wang K (2012) Adsorption of methylene blue from aqueous solution by graphene. Colloids and Surfaces B: Biointerfaces 90:197-203

Lv M, Yan L, Liu C, Su C, Zhou Q, Zhang X, Lan Y, Zheng Y, Lai L, Liu X (2018) Non-covalent functionalized graphene oxide (GO) adsorbent with an organic gelator for co-adsorption of dye, endocrine-disruptor, pharmaceutical and metal ion. Chemical Engineering Journal 349:791-799

McKay G, Sweeney AG (1980) Principles of dye removal from textile effluent. Water, Air, and Soil Pollution 14 (1):3-11

Mercier G, Gleize J, Ghanbaja J, Marêché J-Fo, Vigolo B (2013) Soft oxidation of single-walled carbon nanotube samples. The Journal of Physical Chemistry C 117 (16):8522-8529

Mohandoss M, Gupta SS, Nelleri A, Pradeep T, Maliyekkal SM (2017) Solar mediated reduction of graphene oxide. RSC Advances 7 (2):957-963. doi:10.1039/C6RA24696F

Nassar NN, Marei NN, Vitale G, Arar LA (2015) Adsorptive removal of dyes from synthetic and real textile wastewater using magnetic iron oxide nanoparticles: thermodynamic and mechanistic insights. The Canadian Journal of Chemical Engineering 93 (11):1965-1974

Novoselov KS, Fal'ko VI, Colombo L, Gellert PR, Schwab MG, Kim K (2012) A roadmap for graphene. Nature 490:192. doi:10.1038/nature11458

Pathania D, Sharma S, Singh P (2017) Removal of methylene blue by adsorption onto activated carbon developed from Ficus carica bast. Arabian Journal of Chemistry 10:S1445-S1451. doi:https://doi.org/10.1016/j.arabjc.2013.04.021

Pérez-Ramírez EE, de la Luz-Asunción M, Martínez-Hernández AL, Velasco-Santos C (2016) Graphene materials to remove organic pollutants and heavy metals from water: photocatalysis and adsorption. In: Semiconductor Photocatalysis-Materials, Mechanisms and Applications. InTechOpen,

Polat EO, Balci O, Kakenov N, Uzlu HB, Kocabas C, Dahiya R (2015) Synthesis of Large Area Graphene for High Performance in Flexible Optoelectronic Devices. Scientific Reports 5:16744. doi:10.1038/srep16744

https://www.nature.com/articles/srep16744#supplementary-information

Qi C, Zhao L, Lin Y, Wu D (2018) Graphene oxide/chitosan sponge as a novel filtering material for the removal of dye from water. Journal of colloid and interface science 517:18-27

Qi Y, Yang M, Xu W, He S, Men Y (2017) Natural polysaccharides-modified graphene oxide for adsorption of organic dyes from aqueous solutions. Journal of Colloid and Interface Science 486:84-96. doi:https://doi.org/10.1016/j.jcis.2016.09.058

Qiao X-Q, Hu F-C, Tian F-Y, Hou D-F, Li D-S (2016) Equilibrium and kinetic studies on MB adsorption by ultrathin 2D MoS 2 nanosheets. RSC Advances 6 (14):11631-11636

Robati D, Rajabi M, Moradi O, Najafi F, Tyagi I, Agarwal S, Gupta VK (2016) Kinetics and thermodynamics of malachite green dye adsorption from aqueous solutions on graphene oxide and reduced graphene oxide. Journal of Molecular Liquids 214:259-263. doi:https://doi.org/10.1016/j.molliq.2015.12.073

Selen V, Güler Ö, Özer D, Evin E (2016) Synthesized multi-walled carbon nanotubes as a potential adsorbent for the removal of methylene blue dye: kinetics, isotherms, and thermodynamics. Desalination and Water Treatment 57 (19):8826-8838

Shukla AK, Alam J, Alhoshan M, Dass LA, Ali FAA, Mishra U, Ansari MA (2018) Removal of heavy metal ions using a carboxylated graphene oxide-incorporated polyphenylsulfone nanofiltration membrane. Environmental Science: Water Research & Technology 4 (3):438-448

Stankovich S, Dikin DA, Dommett GH, Kohlhaas KM, Zimney EJ, Stach EA, Piner RD, Nguyen ST, Ruoff RS (2006) Graphene-based composite materials. nature 442 (7100):282

Szlachta M, Wójtowicz P (2013) Adsorption of methylene blue and Congo red from aqueous solution by activated carbon and carbon nanotubes. Water Science and Technology 68 (10):2240-2248

Tahir U, Yasmin A, Khan UH (2016) Phytoremediation: Potential flora for synthetic dyestuff metabolism. Journal of King Saud University-Science 28 (2):119-130

Temkin M, Pyzhev V (1940) Recent modifications to Langmuir isotherms.

Wei D, Liu Y, Zhang H, Huang L, Wu B, Chen J, Yu G (2009) Scalable synthesis of few-layer graphene ribbons with controlled morphologies by a template method and their applications in nanoelectromechanical switches. Journal of the American Chemical Society 131 (31):11147-11154

Yao Y, Xu F, Chen M, Xu Z, Zhu Z (2010) Adsorption behavior of methylene blue on carbon nanotubes. Bioresource technology 101 (9):3040-3046

Yu X, Cheng H, Zhang M, Zhao Y, Qu L, Shi G (2017) Graphene-based smart materials. Nature Reviews Materials 2:17046. doi:10.1038/natrevmats.2017.46

Yusuf M, Elfghi F, Zaidi SA, Abdullah E, Khan MA (2015) Applications of graphene and its derivatives as an adsorbent for heavy metal and dye removal: a systematic and comprehensive overview. RSC Advances 5 (62):50392-50420

Zazouli MA, Azari A, Dehghan S, Salmani Malekkolae R (2016) Adsorption of methylene blue from aqueous solution onto activated carbons developed from eucalyptus bark and Crataegus oxyacantha core. Water Science and Technology 74 (9):2021-2035

Zhao D, Ding Y, Chen S, Bai T, Ma Y (2013) Adsorption of Methylene Blue on Carbon Nanotubes from Aqueous Solutions. Asian Journal of Chemistry 25 (10):5756

Zhao L, Yang S-T, Feng S, Ma Q, Peng X, Wu D (2017) Preparation and Application of Carboxylated Graphene Oxide Sponge in Dye Removal. International journal of environmental research and public health 14 (11):1301. doi:10.3390/ijerph14111301

Zhou X, Zhang Y, Huang Z, Lu D, Zhu A, Shi G (2016) Ionic liquids modified graphene oxide composites: a high efficient adsorbent for phthalates from aqueous solution. Scientific Reports 6:38417. doi:10.1038/srep38417